Clim Dyn (2010) 35:965–975
DOI 10.1007/s00382-009-0632-6

Polar night vortex breakdown and large-scale stirring in the southern stratosphere

Alvaro de la Cámara · C. R. Mechoso · K. Ide · R. Walterscheid · G. Schubert

Received: 18 February 2009 / Accepted: 7 July 2009 / Published online: 23 July 2009

Abstract The present paper examines the vortex breakdown and large-scale stirring during the final warming of the Southern Hemisphere stratosphere during the spring of 2005. A unique set of in situ observations collected by 27 superpressure balloons (SPBs) is used. The balloons, which were launched from McMurdo, Antarctica, by the Stratéole/VORCORE project, drifted for several weeks on two different isopycnic levels in the lower stratosphere. We describe balloon trajectories and compare them with simulations obtained on the basis of the velocity field from the GEOS-5 and NCEP/NCAR reanalyses performed with and without VORCORE data. To gain insight on the mechanisms responsible for the horizontal transport of air inside and outside the well-isolated vortex we examine the balloon trajectories in the framework of the Lagrangian properties of the stratospheric flow. Coherent structures of the flow are visualized by computing finite-time Lyapunov exponents (FTLE). A combination of isentropic analysis and FTLE distributions reveals that air is stripped away from the vortex's interior as stable manifolds eventually cross the vortex's edge. It is shown that two SPBs escaped from the vortex within high potential vorticity tongues that developed in association with wave breaking at locations along the vortex's edge where forward and backward FTLE maxima approximately intersect. The trajectories of three SPBs flying as a group at the same isopycnic level are examined and their behavior is interpreted in reference to the FTLE field. These results support the concept of stable and unstable manifolds governing transport of air masses across the periphery of the stratospheric polar vortex.

Keywords Stratospheric polar vortex dynamics · Vortex breakdown · Large-scale stirring · Finite-time Lyapunov exponents · Hyperbolic manifolds

A. de la Cámara (✉)
Departamento de Geofísica y Meteorología,
Universidad Complutense de Madrid, Madrid, Spain
e-mail: alvarocamara@fis.ucm.es

A. de la Cámara · C. R. Mechoso · K. Ide
Department of Atmospheric and Oceanic Sciences,
University of California, Los Angeles, CA, USA

K. Ide
Department of Atmospheric and Oceanic Science,
University of Maryland, Collage Park, MD, USA

R. Walterscheid
Space Sciences Department, The Aerospace Corporation,
Los Angeles, CA, USA

G. Schubert
Department of Earth and Space Sciences,
Institute of Geophysics and Planetary Physics,
University of California, Los Angeles, CA, USA

1 Introduction

The spring breakdown of the strong cyclonic vortex that characterizes the winter circulation in the middle atmosphere at high-latitudes—and subsequent transition to summer conditions—is referred to as the final warming. During this period, both vertically propagating planetary waves from the troposphere and increased radiative heating as sunlight returns to the polar regions cooperate in decelerating the flow (Yamazaki and Mechoso 1985). In the Southern Hemisphere the large-scale circulation during the final warming shows systematic features, with a strong anticyclone developing over the Indian Ocean and the cyclonic vortex moving off the pole to break down in the upper levels first and in the middle levels later (Mechoso

et al. 1988). Episodes of enhanced planetary wave activity punctuate this systematic evolution, and are often the most interesting dynamical events in a hemisphere without major mid-winter warmings. A very strong event produced a hitherto unobserved split of the southern polar vortex in September 2002; Charlton et al. (2005) proposed that the dynamics implicated in the split involved non-linear dynamics in the coupled troposphere–stratosphere system, and that the notion of forcing from the lower atmosphere could be inadequate.

Studies of the southern stratosphere and analyses of its final warming accelerated after the discovery of the "Antarctic Ozone hole" by Farman et al. (1985). In the consensus view, chemical processes responsible for ozone destruction are initiated both by sunlight and very low temperatures. The right conditions are reached in early spring inside the Antarctic polar night vortex. On an isentropic surface in the lower stratosphere, enhanced potential vorticity (PV) gradients signal the transition to the polar vortex at the approximate location of the westerly jet. Several studies using Lagrangian techniques have conceptually shown how planetary waves propagating and breaking along the vortex edge externally erode the vortex through the formation of filaments (Polvani and Plumb 1992; Waugh and Plumb 1994). This type of erosion is responsible for the formation and continuous regeneration of the enhanced PV gradients that characterize the vortex "edge". According to Bowman (1993), stirring results from repeated stretching and folding of material lines due to planetary wave breaking, and finds much higher stirring rates outside than inside the vortex. Mariotti et al. (2000) examined the ozone "collar" (i.e., the band of maximum values in ozone mixing ratio around the Antarctic ozone "hole") and argued that diabatic descent is responsible for maintaining the local ozone concentrations approximately constant while filaments isentropically disperse collar-like mixing ratios towards lower latitudes. The mechanisms by which air parcels cross the polar vortex edge have been investigated in several studies. Bowman (1996) presents evidence of stirring control in the stratosphere by critical lines, and argues that regions of wave-breaking develop wherein the phase speeds equal the background wind velocity around the austral polar vortex since no waves have phase speeds comparable to the velocities in the jet core. Different arguments have been proposed to explain the formation of barriers to transport: (1) the "PV barrier", which states that large PV gradients are associated with a Rossby restoring force that reduces meridional exchange (Juckes and McIntyre 1987; Dritschel and McIntyre 2008), and (2) the "strong KAM stability", which is based on the existence of a Kolmogorov–Arnold–Moser (KAM) invariant torus that survives in a perturbed system; non-chaotic trajectories on such a torus constitute the transport barrier (Rypina et al. 2007a, 2007b). The former argument leads to the expectation of mixing barriers only on eastward jets, whereas the latter also opens the possibility to westward jets (Beron-Vera et al. 2008).

The present study focuses on the Southern Hemisphere stratosphere during the final warming in 2005. This is a special period because the Stratéole/VORCORE campaign provided a unique set of in situ observations (Hertzog et al. 2007). The project's observational platforms were super-pressure balloons (SPBs) designed to drift in the lower stratosphere on isopycnic surfaces near the pressure levels of either 50 or 70 hPa. Information collected in preparatory exercises with Stratéole balloons have demonstrated the usefulness of SPB datasets for studies on lower stratospheric dynamics. One campaign based in Ecuador provided evidence of mixed Rossby-gravity and Kelvin waves in the equatorial stratosphere (Vial et al. 2001). The data from another campaign based in Kiruna, Sweden, revealed an enhanced contribution to the spectrum of the horizontal wind component by near-inertial waves (Hertzog et al. 2002). VORCORE launched a total of 27 SPBs from McMurdo, Antarctica. These remained inside the stratospheric polar vortex for several weeks. Boccara et al. (2008a) compared VORCORE data of temperature and horizontal wind velocity with those from the National Center for Environmental Prediction/National Center for Atmospheric Research (NCEP/NCAR) reanalysis and the European Centre for Medium-range Weather Forecasts (ECMWF) operational analysis. The ECMWF analysis provides more accurate fields that the NCEP/NCAR reanalysis, although both exhibit an overall temperature bias. Boccara et al. (2008b) provide a method for estimating features of the gravity wave field from quasi-Lagrangian observations, and Hertzog et al. (2008) apply the method to show, using VORCORE data, that almost two-thirds of the total gravity-wave momentum flux can be attributed to waves generated by mountains. In addition, zonally averaged fluxes over the ocean are similar in magnitude to those above the continent, highlighting the importance of non-orographic gravity waves in the Southern Hemisphere.

The present paper uses VORCORE data to gain insight into the motions of air parcels in the stratospheric polar vortex during the southern final warming of 2005. SPBs are constrained to move on isopycnic surfaces and hence they are not perfect tracers of air parcels. However, from September to mid-October the polar vortex is relatively undisturbed and isopycnic surfaces are almost parallel to isentropic surfaces. Therefore, balloon trajectories during that period can be assumed to approximate air parcels trajectories at least for a few days. The approximation also holds after the vortex final breakdown in early December, when the SPBs drifted in the vicinity of the

zero wind level and the waves became evanescent (Hertzog et al. 2007).

We start in Sect. 2 by providing details on the datasets we use. In Sect. 3 we describe the large-scale evolution of the flow based on zonally averaged quantities and deviations from the zonal mean. In the southern spring of 2005, the vortex in the middle stratosphere moved off the pole after an enhancement in the wavenumber-2 component of the flow (wave 2 event), and gradually weakened until it finally disappeared at the end of November. In the lower stratosphere the changes in the zonal-mean quantities proceeded at a slower pace, and the cyclonic circulation remained until early December. Section 4 describes selected features of the balloon trajectories and compares them with trajectories of air parcels simulated by using the velocity field from the GEOS-5 and NCEP/NCAR reanalyses.

The core of the paper is in Sect. 5, where we look into the mechanisms responsible for the horizontal transport of air inside the vortex and across its edge in the framework of Lagrangian coherent structures (LCS) of the flow. Examples of these structures are hyperbolic invariant manifolds, which govern the transport and mixing in dynamical systems: stable and unstable manifolds act as repelling and attracting material lines, respectively (Haller 2002). Figure 1 is a schematic illustration of these properties. When turbulent flows are time-dependent, stable and unstable manifolds can intersect in a so-called hyperbolic trajectory. Two fluid parcels initially close to each other on either side of the stable manifold will approach the hyperbolic trajectory and diverge on either side of the unstable manifold after a sufficiently long period of time. Consequently, invariant manifolds constitute a barrier that fluid particles cannot cross. In this paper we refer to a SPB as located on either the right or left side of a stable manifold according to the view from a point on the stable manifold in the direction toward its intersection with the unstable manifold.

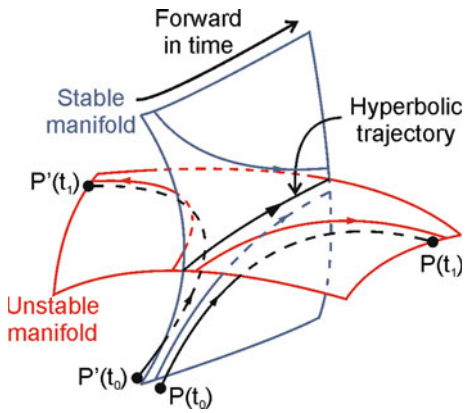

Fig. 1 Behaviour of the hyperbolic trajectory and the trajectories on and near the stable and unstable manifolds. Two trajectories starting from nearby initial conditions across the stable manifolds will diverge after a sufficient time period

To identify the LCS we apply a Lagrangian technique known as finite-time Lyapunov exponents (FTLE). The method quantifies the dispersion rates of fluid parcels by measuring the separation between their trajectories after a predetermined (finite) period. Shadden et al. (2005) provide a numerical method to compute FTLEs, and define LCSs as ridges in their distribution. Haller (2002) examines the accuracy of using FTLEs to extract LCS from a model velocity field. He showed that the invariant manifolds are robust as long as the errors in the model are small according to a special time-weighted norm. Koh and Legras (2002) and Joseph and Legras (2002, JL02 hereafter) visualize the hyperbolic structure of the flow on the Antarctic stratosphere by using the finite-size Lyapunov exponents (FSLE) method. Similar to the FTLE outlined earlier, the FSLE approach quantifies the dispersion rates of fluid parcels based on the period required for the separation between their trajectories to reach a predetermined (finite) length or size. JL02 highlight hyperbolic manifolds in the polar vortex during the southern spring of 1996, and find that the manifolds surrounding the vortex are embedded within a stochastic layer outside the vortex edge (defined as the maximum of the potential vorticity gradient). Their results support the findings by Koh and Plumb (2000) that exchanges of air found by applying lobe dynamics do not occur across the vortex edge, but between the stochastic layer and air at lower latitudes. We have selected to the FTLE method based on our familiarity with it, and our understanding that the results obtained are qualitatively similar to those with FSLE. We emphasize that by using the FTLE method we only seek an approximate determination of the hyperbolic structures of the flow. In this context, the method's usefulness will become evident in a posteriori inspection of observed balloon trajectories.

2 Data sets

2.1 Reanalyses from operational centers

To obtain the hemispheric fields of horizontal wind velocity, temperature and geopotential heights of pressure levels required by our trajectory calculations we use two global reanalyses: (1) NCEP/NCAR (Kalnay et al. 1996), and (2) Goddard Earth Observing System Version 5 (GEOS5) (Reinecker et al. 2007). The former is available four times daily, with a horizontal resolution of 2.5° × 2.5° in longitude and latitude, and 17 levels in the vertical from 1,000 to 10 hPa. The GEOS5 reanalysis is available eight times daily, with a horizontal resolution of 0.66° × 0.5° in

longitude and latitude, and 72 levels in the vertical from 976.6204 to 0.0150 hPa. The use of two reanalyses provides a comparative cross-validation of their accuracy and increases the confidence in our findings.

Furthermore, we have at our disposal two different GEOS5 runs for the southern spring of 2005: the first one incorporates wind data from the VORCORE balloons in the assimilation process (hereafter, GEOS5w); the second run does not contain any VORCORE data and will be referred to as GEOS5wo. The VORCORE information used in GEOS5w is wind data from the SPBs, thinned to one observation each 6 h within a 1° × 1.5° grid box.

2.2 VORCORE data

The VORCORE campaign took place in the southern spring of 2005, when 27 SPBs were launched from McMurdo, Antarctica, during September and October. In order to survey two different constant-density levels in the lower stratosphere (at around 50 and 70 hPa pressure levels) there were two SPB types, one with a 10 m diameter and the other with an 8.5 m diameter. The balloons flew successfully inside the stratospheric polar vortex during an average period of 2 months, recording position, pressure and temperature every 15 min. Position was determined using the global positioning system (GPS). The horizontal wind velocities are derived from successive positions by centered finite differences. The number of balloons simultaneously sampling the polar vortex reached a maximum of 21 at the end of October. The VORCORE observations covered the Antarctic continent and ocean poleward of 55°S. The region sampled varied in time due to displacements of the vortex location during the breakdown process. Hertzog et al. (2007) give a complete description of the VORCORE campaign. Further details can also be found in www.lmd.end.fr/STRATEOLE/.

3 Analysis of the large-scale evolution of the 2005 vortex breakdown

In this section we use the NCEP/NCAR reanalysis, which is perfectly adequate for depicting the large-scale features of the flow. Figure 2a presents a time–height section of the zonal-mean temperature at 65°S, from September to December. A slow but persistent warming is clearly seen in the lower and middle stratosphere from the late winter to the early spring. In the middle stratosphere the warming stops around the second half of November, while in the lower stratosphere continues at a slower rate until the end of December. Figure 2b is a time–latitude plot of the zonal-mean temperature at 20 hPa for the same period as Fig. 2a. The meridional temperature gradient changes sign during the first half of October at this level, thus coinciding with a strong wave 2 event (not shown). A similar sign reversal does not occur in the lower stratosphere until mid-November (not shown).

The behavior of the zonal–mean zonal wind from September to December is displayed in Fig. 3. The zonal flow slows down during the whole period, at a faster rate above 30 hPa, where the zonal flow becomes easterly in mid-November (Fig. 3a). The lower stratosphere shows weak mean easterlies only at the very end of the period. The westerly jet core at 20 hPa is between 55 and 65°S at the beginning of September, with velocities over 60 m/s (Fig. 3b). During the last week of September the strongest zonal winds start to weaken and move slightly poleward. By mid-November the zero wind line is at high latitudes.

The final breakdown of the polar vortex in 2005 broadly shows the systematic evolution identified by Mechoso et al. (1988). This includes development of a strong anticyclone over the Indian Ocean (not shown), erosion of the cyclonic vortex first at the top and later at lower levels, and poleward shift of the zonal-mean jet. The early warming event in the middle stratosphere during the first half of October

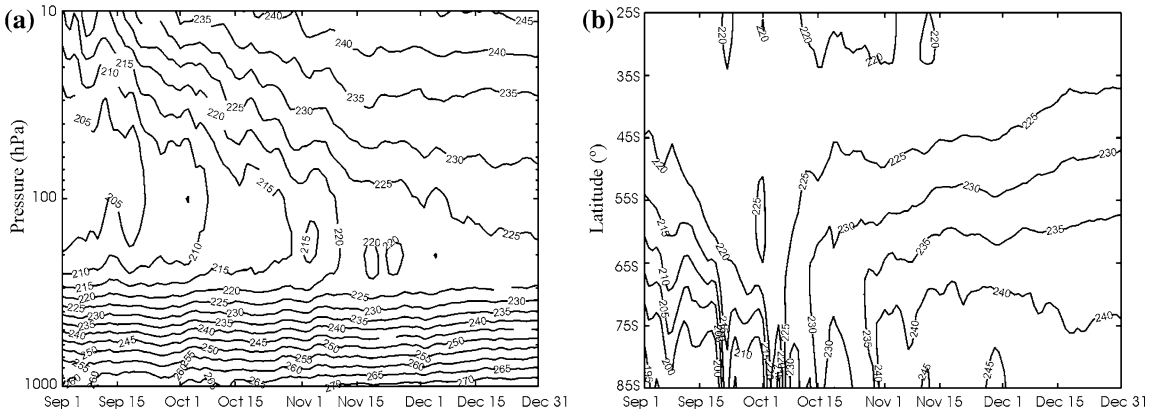

Fig. 2 Time evolution of the zonal-mean temperature from 1 September to 31 December 2005. The contour interval is 5 K. **a** Height–time section at 65S. **b** Latitude–time section at 20 hPa

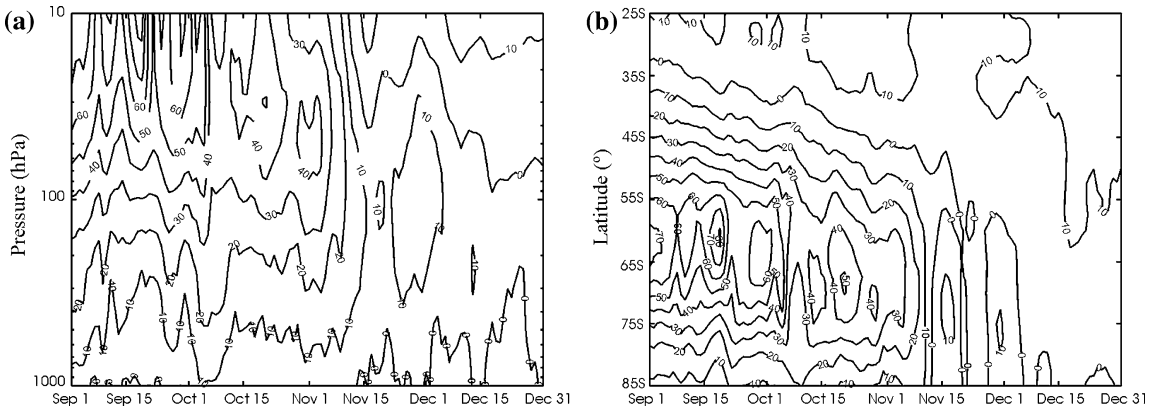

Fig. 3 Time evolution of the zonal-mean zonal wind from 1 September to 31 December 2005. The contour interval is 10 m s^{-1}. **a** Height–time section at 65S. **b** Latitude–time section at 20 hPa

(Fig. 2b), the strong wave 2 event in mid-October (not shown), and the final westerly vortex breakdown in late November together with the onset of the easterly flow (Fig. 3a), closely match one of the two extreme types of spring in the southern stratosphere which Newman (1986) refers to as "early final warming and a strong wave event in mid-October".

4 Simulated balloon trajectories

4.1 Methodology

In this section we present simulated balloon trajectories using velocity fields from the NCEP/NCAR and GEOS5 reanalyses. As explained in a previous section, VORCORE balloons were designed to fly at two different constant-density levels. In order to calculate the simulated trajectories on the same isopycnic levels, we interpolate the horizontal wind—available at pressure levels—to the isopycnic levels upon which the balloons drifted using the following methodology (similar to Boccara et al. 2008a):

- First, the average density at flight level is computed by using the temperature and pressure for the two sets of balloons. The values are 0.0916 kg m^{-3} for the 10 m diameter and 0.1237 kg m^{-3} for the 8.5 m diameter balloons.
- Second, density is calculated at each grid point using temperature data at pressure levels from the reanalysis.
- Finally, wind data are vertically interpolated to the two isopycnic levels at the balloon locations.

The initial conditions for the trajectories were set as close as possible to the initial location of the VORCORE balloons. The velocity field for the advection calculation was linearly interpolated from the reanalysis to the position of the simulated balloons at each time step. For advection, we used a second-order Runge–Kutta integration scheme with a time-step of 3 h during 30 days. The results are insensitive to using a higher order scheme.

4.2 Results

Figure 4 shows the mean spherical distance between actual and simulated balloon positions as function of flight duration, using wind fields from the NCEP/NCAR, GEOS5w and GEOSwo reanalysis. Vertical bars in Fig. 4 indicate the standard deviation (std), computed the following way:

$$\mathrm{std}^t = \sqrt{\frac{\sum_{i=1}^{nb}\left[\left(x_i^t - y_i^t\right) - \left(\overline{x^t - y^t}\right)\right]^2}{\mathrm{nb} - 1}} \qquad (1)$$

where nb is the number of SPBs, x_i^t and y_i^t are the positions of the simulated and actual balloon as a function of time t, respectively, and overbars indicate an average for all the balloons. We note a rapid increase at an almost constant rate during the first ten simulated days, followed by a period of slower growth and more fluctuations. The calculations by Boccara et al. (2008a) using the ECMWF reanalysis show similar behavior. The distances (errors) are larger with the NCEP/NCAR reanalysis, at least during the first 15 days, when distances reach 1,390 ± 925 km at day 5 and 2,090 ± 1090 km at day 10. The corresponding values for GEOS5w are 790 ± 605 km and 2,030 ± 1,450 km, while those for GEOS5wo are 840 ± 570 km and 1,740 ± 1,385 km. Thus, including wind data from the VORCORE balloons in the GEOS5 run has primarily local impacts both in space and time near the balloon trajectories.

The results in Fig. 4 are consistent with the trajectories computed using wind fields from the ECMWF reanalysis versus those from the NCEP/NCAR reanalysis as reported by Boccara et al. (2008a). Hertzog et al. (2004) obtained

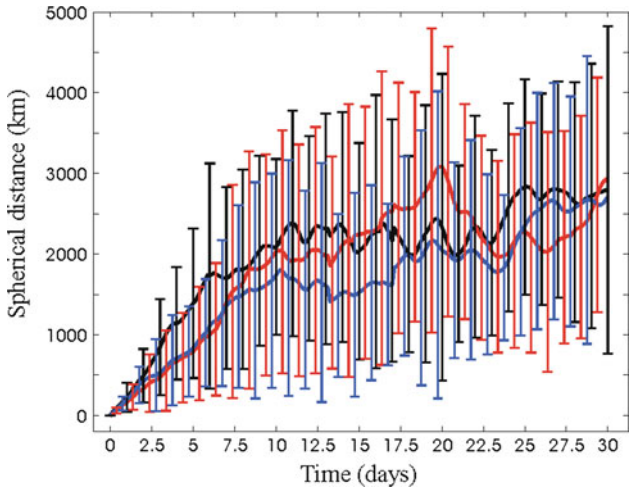

Fig. 4 Mean (*solid lines*) and standard deviation ($\pm$ 1σ) (*error bars*) of the distance between simulated and VORCORE balloon positions as a function of the simulation time. Computed trajectories were calculated using GEOS5w (*red*), GEOS5wo (*blue*) and NCEP/NCAR (*black*) winds

similar results in simulated trajectories in the northern lower stratosphere. The accuracy obtained using both GEOS5 runs is intermediate between the two other reanalysis datasets.

Dvorkin et al. (2001) use a hybrid model for reconstructing four balloon trajectories in the equatorial lower stratosphere. They modify the pure advection model by adding a correction velocity—calculated on the basis of a two-dimensional frictional model—that accounts for the insufficient accuracy of the velocity fields, and find substantial improvement in the computed trajectories. They are cautious, however, in promoting the applicability of their model due to the limited dataset (only four trajectories) and spatial coverage (tropical stratosphere). In the next section we argue that no more refined calculations for parcel trajectories are needed to properly address the goals of the present study.

5 Analysis of selected VORCORE balloon trajectories

In this section we examine selected features in the balloon trajectories in the context of Ertel's potential vorticity and FTLE distributions. This will allow for an assessment of the power of Lagrangian diagnostics in studies of local dispersion properties of turbulent flows. FTLE will help us to identify aspects in the chaotic behavior of the balloons that are not easily explained in an Eulerian framework.

5.1 Methodology for FTLE and PV calculation

Our implementation of the FTLE is as follows. We initialize a reference distribution of parcels on a 0.66° longitude and 0.5° latitude grid over the extratropical Southern Hemisphere on the two isopycnic levels of VORCORE balloons (i.e., 0.0916 and 0.1237 kg/m^3 on average). For each parcel we consider four others at the grid points to the north, west, south and east. Next, each parcel and the four around it are advected forward and backward in time using GEOS5w wind data linearly interpolated in the horizontal and the vertical directions to the parcel positions, as explained in Sect. 4.1. The time step for the calculation is chosen to be 3 h (the results are insensitive to the choice of a shorter time step). To obtain the FTLEs we apply the same methodology as Shadden et al. (2005). Briefly, the method consists of computing the Cauchy-Green deformation tensor and its maximum eigenvalue ($\lambda_{\max}$). This gives:

$$\mathrm{FTLE} = \frac{1}{|T|}\ln\left(\sqrt{\lambda_{\max}}\right) \tag{2}$$

where T is the time interval from the initial to the final position of the parcels, chosen to be 4 days. We have verified that the results using $T = 4$, 6, and 8 days (not shown) are practically identical.

As mentioned in the Introduction, FTLE are not used in the present study to precisely determine hyperbolic manifolds and hyperbolic trajectories. Nevertheless, we will refer to the FTLE maxima as manifolds in this section, and to lines joining FTLE maxima—i.e., where values are above a certain threshold—in the forward (backward) integration as stable (unstable) manifolds. We will justify, a posteriori, that this terminology does not lead to inconsistencies. Moreover, the width of the hyperbolic manifolds visualized by the high FTLE value above the threshold is not representative of the actual width of the kinematic boundaries. Legras et al. (2005) estimated the practical width of the kinematic boundary as a few tens of kilometers based on the ratio of the maximum strain and the diffusion.

Ertel's potential vorticity is calculated in pressure levels (Hoskins et al. 1985)

$$Q = -g(f\vec{k} + \vec{\nabla}_p \times \vec{v}) \cdot \vec{\nabla}_p \theta \tag{3}$$

where Q is PV, g is acceleration of gravity, f is the Coriolis parameter, $\vec{v}$ is the horizontal velocity vector and θ is potential temperature. The values of Q are vertically interpolated to the balloon-flight levels.

5.2 Results

Figure 5 shows the horizontal distribution of PV at the $\rho = 0.0912$ kg/m^3 level, superimposed on the lines joining FTLE values above 0.033 h^{-1} for the forward (blue) and backward (red) integrations for six different times around the end of November and beginning of December

2005. The PV distribution in Fig. 5 depicts a weakened and zonally distorted cyclonic polar vortex centered off the pole. As mentioned in Sect. 3, the north-south temperature gradient has already changed signs in the lower stratosphere by the time considered. On 21 November (Fig. 5a), the region of high PV air is located over Antarctica, but shifted towards the Indian Ocean. Westerly winds are very weak at these levels (Fig. 3a), and vertically propagating waves from the troposphere can easily propagate into the lower stratosphere. An anticyclone developing near the date line over the continent is eroding the cyclonic vortex, and a tongue of high PV air is ejecting from the cyclone's periphery and extending to the date line. The anticyclone strengthens as it reaches higher latitudes, and the tongue of PV air lengthens (Fig. 5b, c). In 25 November (Fig. 5d) the tongue has separated from the main vortex, and debris from this separation is visible around the location 60°W–60°S.

Let us now consider the structure of stable and unstable manifolds in Fig. 5. As pointed out by JL02, the FTLE technique provides a fuzzy description of the manifolds. However, an overall structure clearly emerges, with stable and unstable manifolds surrounding the vortex and intersecting in several locations. The relatively broad appearance of the manifolds impedes a clear view of the complicated tangle of crossings. Nevertheless we do identify main intersections, such as the crossing of a stable and an unstable manifold, from which the high PV air tongue emerges in Fig. 5a and which extends outside the vortex. This feature may indicate the presence of a hyperbolic point in the particular intersection (Haller and Poje 1998; Koh and Plumb 2000).

Figure 5 also shows the location of SPBs number 3 and 27 (SPB-3 and SPB-27, respectively). We will highlight the behavior of these two balloons since they were the only two that managed to escape from the cyclonic vortex

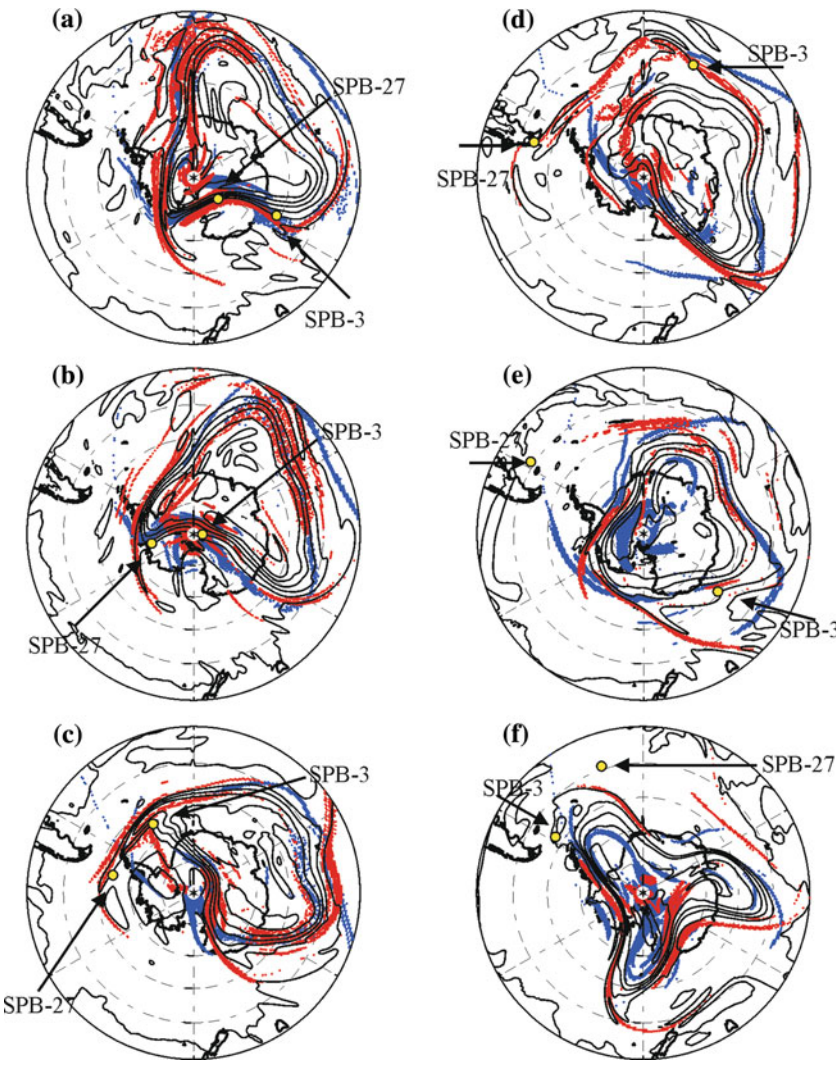

Fig. 5 Contours: potential vorticity maps on the isopycnic level $\rho = 0.0916$ kg m^{-3}. Contour interval 8 PVU (1 PVU $= 10^{-6}$ m^2 s^{-1} kg^{-1} K). *Shaded* Central initial location of set of particles with FTLE values above 0.033 h^{-1}for the forward (*blue*) and backward (*red*) integrations at the same isopycnic level. *Green dots* Location of SPB-3 and SPB-27. **a** 21 November at 06 UTC, **b** 22 November at 06 UTC, **c** 31 November at 18 UTC, **d** 25 November at 18 UTC, **e** 28 November at 09 UTC and **f** 2 December at 00 UTC

before complete breakdown. Let us start with SPB-27, which was ejected outside the vortex through the PV tongue mentioned earlier. We can justify this behavior by the possible location of a hyperbolic trajectory. On 21 November (Fig. 5a) SPB-27 is located at 130.7°E and 79.6°S, which is within a region of high PV gradient that characterizes the vortex edge. We are not able to discern the relative position of the balloon with respect to the unstable and stable manifolds on 21 November, but we can see that it is clearly on the left side of the stable manifold on 22 November (Fig. 5b). An analysis based exclusively on the PV contours would be unclear as to whether the balloon will stay at the vortex edge or will go into the emerging PV tongue. A prediction of behavior can be made by examination of the manifolds. SPB-27 approaches the possible hyperbolic trajectory along the stable manifold and, according to dynamical systems theory, the balloon will move away from the hyperbolic trajectory along the unstable manifold. Hence, SPB-27 will drift along the PV tongue. This is precisely the situation found on 23 November (Fig. 5c).

To our knowledge, this is the first time that results obtained using FTLE—or related Lagrangian analysis tools—are checked against observed trajectories of quasi-Lagrangian tracers in the stratosphere. Even though FTLE are not precise indicators of material barriers for the balloon motions, they give useful hints on the balloon behavior.

We next focus on SPB-3. On 21 and 22 November, this balloon is closely following SPB-27 along the maxima of PV gradient. On 23 November (Fig. 5c) SPB-3 is at the base of the PV tongue along which SPB-27 is escaping. However, SPB-3 and SPB-27 are clearly situated on different regions divided by the manifolds; hence SPB-3 will not exit the vortex on this occasion. On 25 November (Fig. 5d) SPB-3 is still poleward of the region delimited by the intersection of the manifolds, although it is equatorward of the region of high PV gradient. On 28 November (Fig. 5e), another tongue of high PV air is developing around the date line, just in the vicinity of an intersection between a stable and an unstable manifold. The configuration is very similar to that of Fig. 5a. Again, SPB-3 is approaching a tongue on the left side of the stable manifold, and will drift along the unstable branch directly to the PV tongue as shown on the panel corresponding to 2 December (Fig. 5f).

Figure 6 shows plots similar to those in Fig. 5 for four consecutive days in early December. On 3 December the PV field has the imprint of a wave 3 disturbance, which is also discernible in the layout of the manifolds. Figure 6 also shows the positions of three balloons at the same isopycnic level (0.0916 kg m^{-3}), SPB-2, SPB-7 and SPB-15, which on 3 December seem to be drifting as a group. Notably, as we go forward in time (Fig. 6b–d), one of the balloons turns right in its flight and separates from the other two. According to the distribution of FTLE maxima around the group of balloons on 3 December (Fig. 6a), SPB-2 and SPB-7 are located on a stable manifold, but the former is slightly to the right and the latter is a little to the left side of the manifold. SPB-15 is on a different forward FTLE

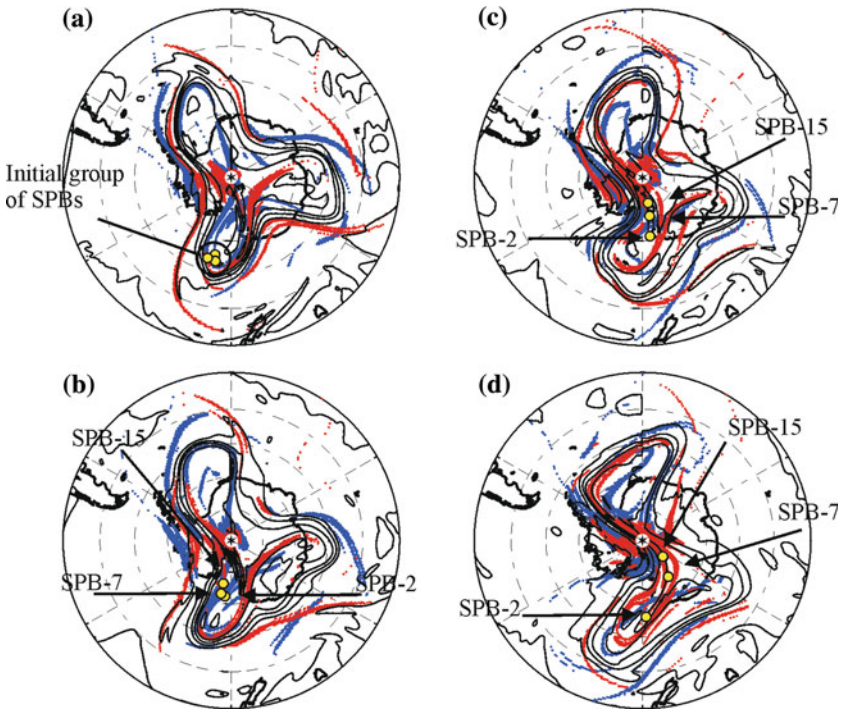

Fig. 6 The same as Fig. 5, but showing the location of SPB2, SPB7 and SPB15. **a** 3 December at 00 UTC, **b** 4 December at 00 UTC, **c** 5 December at 00 UTC and **d** 6 December at 00 UTC

maximum, a bit to the east. The three balloons are clearly inside the region delimited by the maximum PV gradient, and SPB-2 and SPB-7 are both inside a small pool of higher PV air than the surroundings. On 4 December (Fig. 6b) the three balloons are in a region with the same PV, and there is no reason to expect a separation in the group of balloons. However, SPB-2 is slightly on the right of a stable manifold, which separates this balloon from the other two. During the following 2 days (5 and 6 December; Fig. 6c, d), while the PV contours show the progression of the final breakdown of the vortex at this level, SPB-2 stays inside a lobe delimited by intersections of FTLE maxima, whereas SPB-7 and SPB-15 drift away from SPB-2. Both SPB-2 and SPB-7 are still in the same PV region, but have drifted far away from each other. These results provide observational evidence of hyperbolic manifolds delineating different regions of stirring in the Southern Hemisphere stratospheric polar vortex during its final breakdown.

6 Discussion

We have reported two examples of VORCORE SPBs (SPB-3 and SPB-27) that managed to escape from the Antarctic polar vortex (Fig. 5). The flight histories of those balloons are very different from each other. SPB-27 was launched on October 28 already at the vortex edge (high horizontal PV gradient); SPB-3 was released early in the campaign on September 9 and inside the well-isolated vortex of early spring. During September, SPB-3 remains well inside the vortex, following an almost isentropic trajectory since it moves practically along PV contours and isopycnic and isentropic surfaces are nearly parallel to each other. Isopycnic and isentropic surfaces do not remain parallel during October and November due to the progressive warming and the effects of planetary wave disturbances in the lower stratosphere. In this way, SPB-3 could cross PV isolines and approach the vortex edge as a prelude to its escape. From a physical viewpoint, erosion of the vortex by wave disturbances and development of high PV air tongues that are expelled out are the responsible mechanisms for the balloons leaving the vortex. On the other hand, the presence of hyperbolic trajectories does seem to control which balloons succeed in escaping and which do not. Hence, FTLE diagnostics enhances the power of isentropic analysis for a better understanding of the balloons' motions.

Joseph and Legras (2002) provided evidence of a stochastic layer around the vortex, the interior closure of which is the vortex edge. They also showed hyperbolic manifolds—identified by application of the FSLE technique—governing air stirring in this layer, and identified lobe dynamics as the responsible mechanism for injection of air from the stochastic layer to lower latitude areas and vice versa. Although JL02 did not directly address the kinematic mechanisms at work for the transport across the vortex edge, they hypothesized that the stochastic layer and its interior closure (the vortex edge) need to be defined over time intervals short enough for isentropic advection to dominate over diffusion and diabatic processes (in our case, isentropic advection will always dominate over molecular diffusion for the resolved spatial scales). They stated that from one of these intervals to the next, parts of the new stable manifolds may lie inside the previously isolated vortex and thus vortex air might be incorporated into the stochastic layer. Our results in Fig. 5 support this hypothesis. SPB-27 flies along the vortex edge—high PV gradients—for several days (not shown), but it is not until the stable manifold intrudes into this region that the balloon leaves the vortex.

Our success in applying FTLE to study observed balloon trajectories suggest that the accuracy of the trajectory calculations (Sect. 4) is adequate for the calculation of FTLE. Haller (2002) concludes that errors in individual particle trajectories will spread along hyperbolic manifolds, but errors transverse to hyperbolic manifolds remain small. This is to say that true and computed material lines will not separate exponentially though true and computed trajectories may do so. In the present paper there has been no discrimination between maximized FTLE and hyperbolic manifolds. Even so, it has been shown that this discrimination is not required since there is good agreement between balloon trajectories and the FTLE distribution. Therefore, an improvement in the trajectory computations—i.e., a higher order scheme of integration, shorter time step for the integration or the use of a more complex model for balloon motion as in Dvorkin et al. (2001)—might lead to a more realistic representation of the motions of individual fluid parcels, but it would not necessarily change the general structure of the hyperbolic manifolds.

7 Summary and conclusions

We have investigated the vortex breakdown in the southern stratosphere during the spring of 2005. A large-scale analysis of the final warming has been performed by means of zonally averaged quantities—zonal wind and temperature. The results indicate that persistent zonal mean easterlies at high latitudes do not appear in the middle stratosphere until December, whereas the reversal of the latitudinal temperature gradient already occurs during the first half of October.

Our main goal has been the better understanding of the control exerted by the polar vortex on the motion of air parcels during the process of vortex weakening and

breaking. We made use of a unique set of in situ observations of the lower stratosphere provided by the Stratéole/VORCORE superpressure balloons that drifted on isopycnic surfaces in the Antarctic region for several months. Simulated balloon trajectories using horizontal wind data at isopycnic levels from NCEP/NCAR, GEOS5w and GEOS5wo reanalysis were obtained and compared with the observed trajectories. The results showed a rapid increase in the distance between simulated and actual balloon locations during the first 10 days, followed by a period of fluctuations. These findings are in agreement with Trounday et al. (1995). The accuracy of our trajectories computed with GEOS5 is intermediate between ECMWF—the best accuracy—and NCEP/NCAR reanalyses, in agreement with Boccara et al. (2008a).

Selected balloon trajectories were analyzed using a combination of potential vorticity diagnostic and FTLE at isopycnic levels. FTLE are used to determine approximate locations of maximum divergence of air parcel trajectories, and hence to broadly identify hyperbolic manifolds in the lower stratospheric flow. To our knowledge, this is the first time that FTLE have been successfully used to analyze observed trajectories in the stratosphere.

We have shown that two SPBs escaped from the vortex inside tongues of high PV vortex air ejected from its periphery. The tongues developed in the region where an anticyclone erodes the vortex, and they are thus interpreted as a signature of wave breaking. In addition, the ejections occur in the intersection of forward and backward FTLE maxima (approximately stable and unstable manifolds, respectively), indicating the presence of a hyperbolic trajectory. For the ejection of SPB-27, the flow evolves in such a way that the stable manifold slightly crosses the edge of the vortex in the location where SPB-27 is positioned. SPB-27, therefore, moves away from the hyperbolic trajectory along the unstable manifold inside the high PV air tongue. This result supports JL02's contention that a stable manifold, usually located in the outside surroundings of the vortex edge (in the "stochastic layer"), may lie inside the vortex and take out air from inside.

We have also reported an example of manifolds delimiting different regions of stirring when the vortex is breaking down in the lower southern stratosphere (Fig. 6). In this regard we examined the trajectories of three balloons flying as a group at the same isopycnic level. At some point in time one of the balloons separates from the other two. Our FTLE calculations using analyzed winds are successful in locating the three balloons on different mixing regions separated by hyperbolic manifolds.

A number of studies have applied FTLE or related techniques to identify LCS and investigate transport and stirring in the stratosphere and the ocean (d'Ovidio et al. 2004; Lehahn et al. 2007; Waugh and Abraham 2008). Some of these studies have used indirect observational evidence to support the conclusion that the calculation of manifolds using reanalysis products is useful for analyzing real trajectories. For example, Bowman et al. (2007) calculated invariant manifolds in the upper troposphere and successfully contrasted them with the distribution of in situ and satellite measurements of different constituents (water vapor, ozone, etc.). To our knowledge, the present paper is the first to verify the calculations from manifolds against observed trajectories of quasi-Lagrangian tracers in the stratosphere. These results have implications for the better understanding of the dynamics of the polar vortex isolation, which is an integral component of the Antarctic ozone hole formation.

Acknowledgments The authors especially thank Andrew V. Tangborn, from the National Aeronautics and Space Administration (NASA), for providing with the GEOS5 data and Lynette J. Gelinas for helpful discussion. The authors are also grateful to the two anonymous reviewers for their constructive and useful comments that help improve the manuscript. VORCORE was jointly supported by Centre National de la Reserche Scientifique (CNRS), France, the Centre National d'Études Spatiales (CNES), France, and the National Science Foundation (NSF), USA. The research was supported by NSF Grant ATM—0732222 and by Office of Naval Research Grants N00014040191 and N000140910418 and by the Spanish Ministry of Science and Innovation project CGL2008-06295.

References

Reinecker MM et al (2007a) The GEOS-5 data assimilation system: a documentation of GEOS-5.0, in Tech. Rep. 104606 V27, NASA. Internal communication

Beron-Vera FJ, Brown MG, Olascoaga MJ, Rypina II, Koçak H, Udovychenkov IA (2008) Zonal jets as transport barriers in planetary atmosphere. J Atmos Sci 65:3316–3326

Boccara G, Hertzog A, Basdevant C, Vial F (2008a) Accuracy of NCEP/NCAR reanalyses and ECMWF analyses in the lower stratosphere over Antarctica in 2005. J Geophys Res. doi: 10.1029/2008JD010116

Boccara G, Hertzog A, Vincent RA, Vial F (2008b) Estimation of gravity-momentum flux and phase speeds from quasi-Lagrangian stratospheric balloon flights. 1: theory and simulations. J Atmos Sci 65:3042–3055

Bowman KP (1993) Large-scale isentropic properties of the Antarctic polar vortex from analyzed winds. J Geophys Res 98:23013–23027

Bowman KP (1996) Rossby wave phase speeds and mixing barriers in the stratosphere. Part I: observations. J Atmos Sci 53:905–916

Bowman KP, Pan LL, Campos T, Gao R (2007) Observations of fine-scale transport structure in the upper troposphere from the high-performance instrumented airborne platform for environmental research. J Geophys Res 112:D18111. doi:10.1029/2007JD008685

Charlton AJ, O'Neill A, Lahoz WA, Berrisford P (2005) The splitting of the stratospheric polar vortex in the Southern Hemisphere, September 2002: dynamical evolution. J Atmos Sci 62:590–602

d'Ovidio F, Fernández V, Hernández-García E, López C (2004) Mixing structures in the Mediterranean Sea from finite-size Lyapunov exponents. Geophys Res Lett 31:L17203. doi: 10.1029/2004GL020328

Dritschel DG, McIntyre ME (2008) Multiple jets as PV staircases: the Phillips effect on the resilience of eddy-transport barriers. J Atmos Sci 65:855–874

Dvorkin Y, Paldor N, Basdevant C (2001) Reconstructing balloon trajectories in the tropical stratosphere with a hybrid model using analysed fields. Q J R Meteorol Soc 127:975–988

Farman JC, Gardiner BG, Shanklin JD (1985) Large losses of total ozone in Antarctica reveal seasonal ClO_x/NO_x interaction. Nature 315:207–210

Haller G (2002) Lagrangian coherent structures from approximate velocity data. Phys Fluids 14:1851–1861

Haller G, Poje AC (1998) Finite time transport in aperiodic flows. Phys D 119:352–380

Hertzog A, Vial F, Mechoso CR, Basdevant C, Cocquerez P (2002) Quasi-Lagrangian measurements in the lower stratosphere reveal an energy peak associated with near-inertial waves. Geophys Res Lett 29:1229. doi:10.1029/2001GL014083

Hertzog A, Basdevant C, Vial F, Mechoso CR (2004) The accuracy of stratospheric analyses in the Northern Hemisphere inferred from long-duration balloon flights. Q J R Meteorol Soc 130:607–626

Hertzog A, Cocquerez P, Basdevant C, Boccara G, Bordereau J, Brioit B, Cardonne A, Guilbon R, Ravissot A, Schmitt E, Valdivia JN, Venel S, Vial F (2007) Strateole/VORCORE—long-duration, superpressure balloons to study the Antarctic lower stratosphere during the 2005 winter. J Atmos Oceanic Technol 24:2048–2061

Hertzog A, Boccara G, Vincent RA, Vial F (2008) Estimation of gravity–momentum flux and phase speeds from quasi-Lagrangian stratospheric balloon flights. 2: results from the VORCORE campaign in Antarctica. J Atmos Sci 65:3056–3070

Hoskins BJ, McIntyre ME, Robertson AW (1985) On the use and significance of isentropic potential vorticity maps. Quart J R Meteorol Soc 111:877–946

Joseph B, Legras B (2002) Relation between kinematic boundaries, stirring, and barriers for the Antarctic polar vortex. J Atmos Sci 59:1198–1212

Juckes NM, McIntyre ME (1987) A high-resolution one-layer model of breaking planetary waves in the stratosphere. Nature 328:590–596

Kalnay E et al (1996) The NCEP/NCAR 40-year reanalysis project. Bull Am Meteorol Soc 77:437–471

Koh T-Y, Legras B (2002) Hyperbolic lines and the stratospheric polar vortex. Chaos 12:382–394

Koh T-Y, Plumb RA (2000) Lobe dynamics applied to barotropic Rossby-wave breaking. Phys Fluids 12:1518–1528

Legras B, Pisso I, Berthet G, Lefèver F (2005) Variability of the Lagrangian turbulent diffusion in the lower stratosphere. Atmos Chem Phys 5:1605–1622

Lehahn Y, d'Ovidio F, Léyy M, Heifetz E (2007) Stirring of the northeast Atlantic spring bloom: a Lagrangian analysis based on multisatellite data. J Geophys Res 112:C08005. doi:10.1029/2006JC003927

Mariotti A, Mechoso CR, Legras B, Daniel V (2000) The evolution of the ozone "collar" in the Antarctic lower stratosphere during early August 1994. J Atmos Sci 57:402–414

Mechoso CR, O'Neill A, Pope VD, Farrara JD (1988) A study of the stratospheric final warming of 1982 in the southern hemisphere. Q J R Meteorol Soc 114:1365–1384

Newman PA (1986) The final warming and the polar vortex disappearance during the Southern Hemisphere spring. Geophys Res Lett 13:1228–1231

Polvani LM, Plumb RA (1992) Rossby wave breaking, microbreaking, filamentation and secondary vortex formation: the dynamics of a perturbed vortex. J Atmos Sci 49:462–476

Rypina II, Brown MG, Beron-Vera FJ, Koçak H, Olascoaga MJ, Udovydchenkov IA (2007a) On the Lagrangian dynamics of atmospheric zonal jets and the permeability of the stratospheric polar vortex. J Amos Sci 64:3595–3610

Rypina II, Brown MG, Beron-Vera FJ, Koçak H, Olascoaga MJ, Udovydchenkov IA (2007b). Robust tranport barriers resulting from strong Kolmogorov–Arnold–Moser stability. Phys Rev Lett 98:104102. doi:10.1103/PhysRevLett.98.104102

Shadden SC, Lekien F, Marsden JE (2005) Definition and properties of Lagrangian coherent structures from finite-time Lyapunov exponents in two-dimensional aperiodic flows. Phys D 212:271–304

Trounday B, Perthuis L, Strebelle S, Farrara JD, Mechoso CR (1995) Dispersion properties of the flow in the southern stratosphere during winter and spring. J Geophys Res 100:13901–13917

Vial F, Hertzog A, Mechoso CR, Basdevant C, Cocquerez P, Dubourg V, Nouel F (2001) A study of the dynamics of the equatorial lower stratosphere by use of ultra-long-duration balloons, 1: planetary scales. J Geophys Res 106:22725–22743

Waugh DW, Abraham ER (2008) Stirring in the global surface ocean. Geophys Res Lett 35:L20605. doi:10.1029/2008GL035526

Waugh DW, Plumb RA (1994) Contour advection with surgery: a technique for investigating finescale structure in tracer transport. J Atmos Sci 51:530–540

Yamazaki K, Mechoso CR (1985) Observations of the final warming in the stratosphere of the Southern Hemisphere during 1979. J Atmos Sci 42:1198–1205